EFFECT OF THE NUMBERS OF SLOTS AND BARRIERS ON THE OPTIMAL DESIGN OF SYNCHRONOUS RELUCTANCE MACHINES

Marco PALMIERI Maurizio PERTA Francesco CUPERTINO
DEI - Department of Electrical and Information Engineering, Politecnico di Bari, Italy
TEL: +390805963769, EMAIL: marco.palmieri@poliba.it, maurizio.perta@gmail.com, francesco.cupertino@poliba.it

Gianmario PELLEGRINO
DENERG – Energy Department, Politecnico di Torino, Italy
TEL: +390110907143, EMAIL: gianmario.pellegrino@polito.it

Abstract *— This paper analyzes the impact of the numbers of stator slots and rotor layers on the optimal design of synchronous reluctance (SyR) machines. Eighteen SyR machine examples have been designed by means of a multi-objective optimization algorithm and finite element analysis so to maximize torque and minimize torque ripple. Twelve, twenty-four and forty-eight slot stators are considered, associated to rotors with four-poles and one to six flux barriers per pole. The results of the comparative analysis show that high numbers of slots and layers are beneficial for maximizing the torque and the power factor, and that torque ripple and iron loss minimization require precise matches between the slots and the layers, which are not necessarily the same for the two purposes. Finally, for some slot/layer combinations the optimization algorithm produces nonconventional barrier distributions, very promising is some cases. A fast finite element evaluation is used for the evaluation of thousands of candidate machines during the optimization, whereas an accurate transient with motion finite element analysis stage is used for the off-line characterization of the final designs.*

Key words *— Synchronous Reluctance Machines, Rotor design, Design Optimization, Pareto Optimization, Torque Ripple Minimization, Maximum Torque per Ampere, Electrical Machine Design, Automated Design.*

I. INTRODUCTION

Synchronous Reluctance (SyR) motors are a viable alternative to inverter-driven induction motors (IMs) because of their higher efficiency, lower rotor temperature and superior transient overload capability. SyR machines have been studied extensively in the 1990s [1-5] and recently reconsidered by major manufacturers [6], due to the increasingly restrictive efficiency standards for energy saving motors and the appealing absence of permanent magnets and windings on the rotor.

The design of transverse laminated, segmented SyR machine rotors was formalized through the years with different approaches to the shape of the rotor flux barriers and their optimization [3,5-6]. Finite element analysis (FEA) is adopted by all authors, including the ones that base their design mostly on analytical models [1-3,6-7], because neglecting the magnetic saturation effects would produce non-realistic overestimates of saliency and torque [1].

In this paper the SyR machines are designed automatically via the joint use of a multi-objective optimization algorithm (MOOA) and finite-element analysis (FEA). Previous works addressed how the multi-barrier rotors can be described with a limited number of variables and how FEA can be used efficiently for the quick evaluation of numerous candidate solutions. During the optimization, a single current condition and few rotor positions are sufficient to evince the torque and torque ripple capability of each new machine. Parallel processing contribute to shorten the computational time [8]. Different optimization algorithms were compared in [9], all producing competitive machines, validated experimentally.

The aim of the paper is twofold: 1) to evaluate the effects of the number of rotor layers and stator slots on the machine performance comprehensively, including core losses, drawing conclusions that are independent from the adopted design procedure; 2) to put in evidence that some of the slot/layer

combinations that are considered not promising by the literature force the optimization algorithm to find nonconventional barrier distributions, and to verify where they can have a potential.

In the literature it is shown that a high number of layers has beneficial effects on the output torque and power factor, and that also high numbers of stator slots are effective in this sense [1]. When torque ripple is considered, the number of layers must be properly matched to the number of stator slots [5]. Similar conclusions about torque and torque ripple are drawn in a more recent comparative study [10]. Still, the crucial aspect of iron loss was not addressed with the same accuracy for this type of machines. In [11] it is stated that axially laminated rotors produce extra rotor loss and in [12] it is shown how such loss is related to the stator slot number and shape. Other papers address loss minimization for PM-assisted SyR [13] and interior PM machines with one or two barriers [14-15].

This paper proposes a comparative study of different stator/rotor combinations from both torque and iron losses points of view. Multi-Objective Differential Evolution (MODE) algorithm [16] is applied to rotor optimization of example SyR motors of small size, with a rated speed of 5000 rpm and maximum speed of 8000 rpm. Three stators, having respectively 12, 24 and 48 slots, are combined with six different rotors, with one to six barriers per pole. The stator geometry optimization is out of the scope of this study. The rotors are optimized individually for each stator, for a total of 18 example machines with 18 different rotors. Each machine is the result of a torque and torque ripple optimization process, carried out by the MODE algorithm. The MODE design takes advantage of the cited fast magneto-static FE analysis for the quick evaluation of thousands of solutions. Afterwards, each of the 18 optimal machines is re-evaluated more accurately by means of transient FE simulations, including the evaluation of iron losses and efficiency.

Finally, general conclusions on the comparison are drawn. The results of the analysis are in line with the design rules in the literature for what concerns the choice of the numbers of slots and layers for torque maximization, as well as for the positioning of the layers for torque ripple minimization. Furthermore, the results of the paper integrate iron loss considerations within the torque – torque ripple comparative framework and present unconventional design choices that can improve the final performance.

II. AUTOMATED SYR MACHINE DESIGN

A. Rotor Geometry and Parameterization

In the design of SyR motors, the most critical part is the determination of the rotor geometry which heavily affects the final performance in terms of torque, torque ripple and losses [1-6,13-15]. The most important rotor parameters are 1) the number of flux barriers, 2) their position at the airgap and 3) the alternation of flux barriers and flux guides thicknesses.

In previous works each rotor barrier was described by two parameters: the angular position of its ends at the airgap and its radial thickness. Barriers of circular and angled shapes were tested [8], with comparable results. In this paper one more degree of freedom per barrier is included, to account for the thickness of the flux guides separately from the thickness of the flux barriers.

The automatic construction of the flux barriers was embedded into the optimization procedure by means of the Matlab scripting feature of FEMM [17]. The field lines of a virtual solid rotor, reported in Fig. 1, are used as guidelines for the barrier side profiles. A closed form expression of such field lines can be derived from the conformal mapping theory and the Joukowski air-flow potential formulation [16]. This was originally developed to describe the fluid flow paths channeled by two infinite plates forming an angle π/p and with a plug of radius a centered into the origin of the reference frame as represented in Fig. 1. In the solid rotor context, the plug represents the nonmagnetic shaft. The equation expressing magnetic field potential lines of Fig 1 is:

$$C = sin(p\vartheta) \cdot \frac{\left(\frac{r}{a}\right)^{2p} - 1}{\left(\frac{r}{a}\right)^{p}} \quad (1)$$

where r and θ (radius and polar angle) are the polar coordinates of each point of the plane, p is the number of pole pairs of the machine, a is the shaft radius. C is a constant that defines which field line is considered: the lower it is, the closer the corresponding field line is to the shaft. Therefore, the field lines can be selected with continuity by the proper choice of C and each line corresponds to a single value of C. For example, to pick up the field line that intercepts the airgap at a given angular

coordinate α_k, the value C_k is determined by substitution of the coordinates of point E_k (r_k, θ_k), as shown in Fig. 1 (E stands for end-point). Once C_k is known, the explicit equation of the field line, in polar coordinates, is:

$$r(\vartheta, C) = a \cdot \sqrt[p]{\frac{C+\sqrt{C^2+4sin^2(p\vartheta)}}{2sin(p\vartheta)}} \quad 0 \le \vartheta \le \frac{\pi}{p} \quad (2)$$

B. *Automated Construction of One Barrier*

The MODE algorithm selects, for the k-th barrier, three parameters: the angular position α_k, the barrier thickness hc_k and the offset of the barrier from its center line Δfe_k.

At first, the angular position α_k defines the center line of the k-th flux barrier, as just described. Once the nominal midline is fixed, the two sides of the flux barrier are determined according to hc_k and Δfe_k as described in the following. M_k is the mid-point of the center line and its coordinates are $(r_{Mk}, \frac{\pi}{2p})$. The radius r_{Mk} is obtained by substitution of C_k and $\vartheta = \frac{\pi}{2p}$ into (2). After M_k, the mid-points of the inner and outer bounds of the barrier (B_{1k}, B_{2k}) are fixed according to:

$$r_{B1,k} = r_{Mk} - \frac{hc_k}{2} \cdot (1 - \Delta fe_k) \qquad \vartheta = \frac{\pi}{2p} \quad (3)$$

$$r_{B2,k} = r_{Mk} + \frac{hc_k}{2} \cdot (1 + \Delta fe_k) \qquad \vartheta = \frac{\pi}{2p} \quad (4)$$

where the per-unit offset factor Δfe_k varies in the range [-1, 1]. Now the inner and outer bounds are constrained, as they are the field lines passing by B_1 and B_2. The substitution of the coordinates of B_1 and B_2 into (1) and the application of (2) permit to trace the flux barrier sides. The procedure is graphically represented in Fig. 2.

The resulting barrier is then thick hc_k along the q-axis and less elsewhere; it is offset outwards or inwards respect to its nominal midline (the one defined by α_k and E_k) according to Δfe_k . For example, if Δfe_k = 1 the barrier is 100% offset outwards and its inner bound coincides with the nominal midline; vice-versa with Δfe_k = -1.
If Δfe_k = 0 the barrier is equally split around the nominal midline.

The structural ribs connecting the flux guides at the air-gap are traced using two circular segments tangent to the barrier boundary line on one end and parallel to the rotor external circumference at angular position α_k.

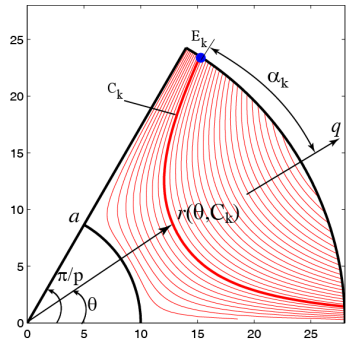

Fig. 1. Field lines in a solid rotor according to conformal mapping.

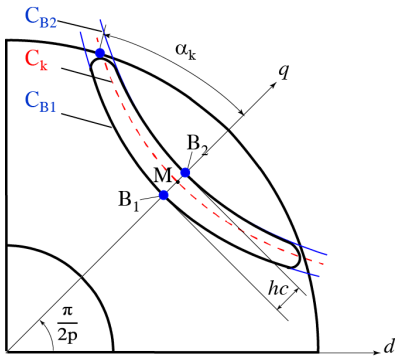

Fig. 2. Construction of the rotor flux barriers according to geometric input.

C. *Automated Construction with Multiple Barriers*

When multi-barrier rotors are considered, some coordination of the input data of each barrier is necessary to avoid overlap of the barriers traces and combinations of the inputs leading to unfeasible rotors. At this purpose, the angles and thicknesses are expressed in normalized quantities, so that their respective sums do not exceed the available angular span (π/2p) and the available space along the q-axis, respectively. Moreover, a minimum clearance of 1 mm is guaranteed between adjacent barriers to ensure that the steel flux guides are at least 1 mm thick and then physically feasible.

A width of 0.4 mm was used for all the inter-layer ribs during the optimization. All the designed machines have been verified towards centrifugal stress via structural FEA, at the maximum speed of 8000 rpm.

D. Common Ratings of the Machines Under Comparison

The definition of the main geometric parameters followed a preliminary study, developed on the basis of the minimal target specifications reported in Table I and the minimum required torque/power profiles in Fig. 3. All the stators (12, 24 and 48 slots) have an outer diameter of 101 mm and the same bore diameter. The rotor diameter is 58.58 mm for all rotors and the airgap length is 0.5 mm. The axial length of the stack is 65 mm for all machines. For each stator, six rotors were designed, having from 1 to 6 rotor barriers per pole, for a total of 18 different rotors. It is worth noticing that the slot geometries of the three stators and the number of turns are designed so to have the same phase resistance for all the machines. In this way the current amplitude defines the amount of Joule loss.

TABLE I - Common Target Values

Continuous output power	2 kW
Rated speed	5000 rpm
Maximum speed	8000 rpm
DC-bus voltage	140 V
Efficiency*	> 85%
Torque ripple*	< 10%
Current density	< 10 A/mm^2
Allowed copper losses	200 W
Number of poles	4
* in the constant power region	

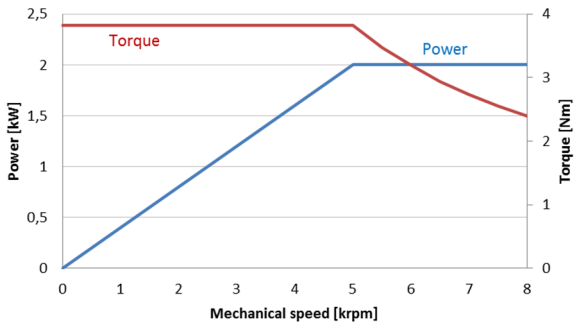

Fig. 3. Torque and Power envelope.

E. Rotor Optimization and Performance evaluation

The workflow of the automated design procedure consists of two consecutive steps:

1. rotor geometry optimization: MODE optimization of average torque and torque ripple via magneto-static FEA simulations, using Matlab and FEMM [17].
2. motor performance evaluation: torque profile and iron losses calculation via transient FEA with MagNet by Infolytica [18].

The already introduced input variables ($\Delta\alpha_k$, hc_k, Δfe_k) form a set of $3n_{lay}$ inputs, where n_{lay} is the number of flux barriers per pole. As suggested in [8-9], the current phase angle γ in the dq frame is included among the parameters optimized by the MODE, in order to estimate Maximum torque per Ampere (MTPA) angle without additional simulations. The overall number of variables to be optimized is then $3n_{lay}+1$. The range of the input parameters is reported in Table II.

Each rotor optimization was performed running five times the MODE algorithm and selecting the best machine from the aggregate of the five torque versus torque ripple Pareto fronts. During optimization process, the current amplitude has been set to twice the machine rated current, as machines with a good behavior in terms of torque ripple in overload conditions, generally show satisfying performances also at rated current. For example, Fig. 4 reports the five Pareto fronts for the 24/3 case, intended as 24 slots, 3 layers per pole. More details on the five step MODE procedure can be found in [9].

TABLE II
LIMITS OF THE SEARCH SPACE FOR THE MODE OPTIMIZATION

Parameter	Min value	Max value	Units
hc_i	0.2	1	p.u.
Δfe_i	-1	1	p.u.
$\Delta\alpha_1$	12	27	degrees
$\Delta\alpha_i$ $(i\neq1)$	0.33	0.67	p.u.
γ	20	80	degrees
i = 1 ÷ 6 (number of rotor barriers)			

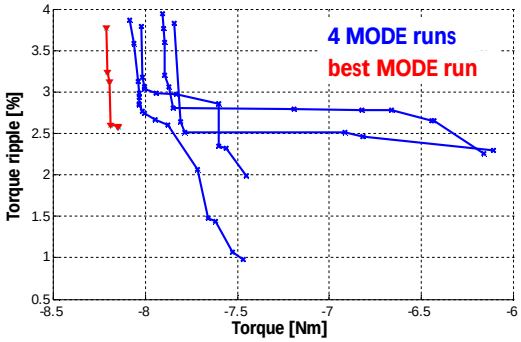

Fig. 4. Pareto fronts of the five MODE runs dedicated to the 24/3 case.

F. *Accurate Evaluation of the Final Designs*

Each of the 18 final machines was re-evaluated with the Transient-with-Motion analysis of MagNet by Infolytica. Each considered (i_d, i_q) condition was simulated in 180 rotor positions over one electrical period to obtain an accurate evaluation of iron loss in the stator and in the rotor.

Different operating conditions were simulated and the results presented here refer to three key combinations: 1) rated current, rated speed (I_n, 5000 rpm); 2) 100% overload current, rated speed ($2I_n$, 5000 rpm); 3) rated current, maximum speed (I_n, 8000 rpm).

The rated speed simulations refer to the respective MTPA current angles, FEA evaluated. For the simulations at 8000 rpm the current phase angle is advanced with respect to the MTPA value so to have constant power versus speed for all machines. It was verified for all the machines that the voltage limit was always respected in this flux weakening condition. To summarize: two current levels and two speeds are comparatively investigated. Joule loss are the same for all the machines, given the current amplitude.

After these simulations the torque waveforms, the iron losses in the stator and the rotor cores and the efficiency have been determined for each machine.

III. RESULTS

The first set of results deals with torque and torque ripple analysis. The second one is related to iron losses and efficiency study. The third part of this section discusses the final geometries of the MODE optimized machines and compares the results with the geometrical rules suggested by the related literature. Finally, detailed results of the torque analysis both in time and frequency domains for 4 optimized machines are reported.

A. *Torque - Torque Ripple Optimization Results*

Fig. 5 and Fig. 6 show the average torque values at rated speed at I_n and $2I_n$, for all the optimized machines. For any given number of rotor barriers, the higher is the stator slots number, the higher is the mean torque value. From a different standpoint the single layer rotors are evidently noncompetitive and, for a fixed number of stator slots, increasing the layer number improves the output torque, mildly but consistently.

As regards torque ripple behavior, according to both Fig. 5 and Fig. 6, each stator has a preferred number of rotor barriers that allows ripple minimization. In 12 and 24 slots motors torque ripple is minimized choosing a rotor with 5 barriers per pole, while in 48 slots machines it is minimized selecting a lamination with 6 barriers per pole. As for the average torque, higher numbers of stator slots are generally better than lower numbers also in terms of torque ripple. The machines with more slots produce a lower magneto-motive-force (MMF) harmonic content, thus making it easier to minimize the torque ripple. Also for torque ripple, the single layer designs perform poorly.

The comparison of Fig. 5 and Fig. 6 shows that machines with better torque and torque ripple figures at rated current tend to perform well also in overload conditions.

Fig. 7b shows torque ripple trend at rated current and maximum speed. By comparing Fig. 5b and Fig. 7b, it can be noticed that torque ripple generally increases passing from constant torque region to constant power region (i.e. moving away from the MTPA trajectory). This agrees with [8-9], where it was observed that the MTPA and the minimum torque ripple trajectories tend to coincide, when the proposed design approach is used.

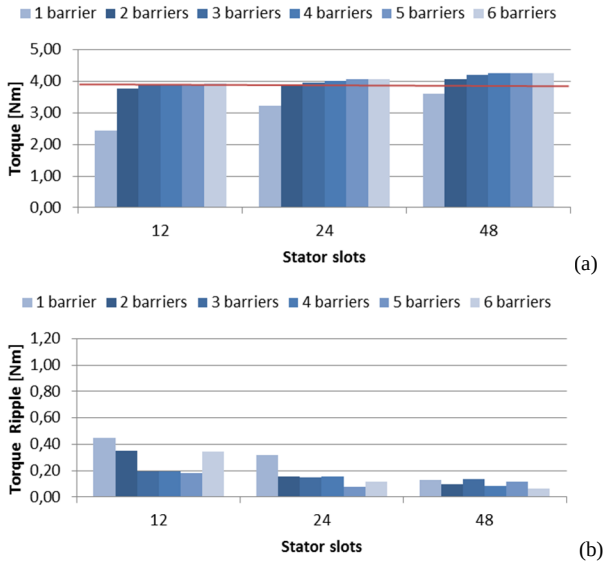

Fig. 5. Average torque (a) and standard deviation of torque ripple (b) at rated current and rated speed (5000 rpm).

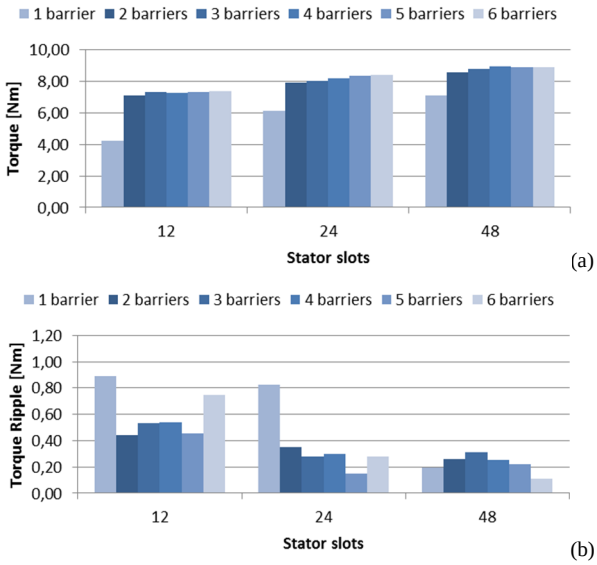

Fig. 6. Average torque (a) and standard deviation of torque ripple (b) at twice rated current and rated speed (5000 rpm).

To conclude, from the torque – torque ripple standpoint:

1. the number of stator slots should be possibly maximized;
2. the number of layers must be chosen according to the number of slots for torque ripple minimization; this does not harm the average torque value;
3. single layer rotors are avoided, as indicated by their poor output figures.

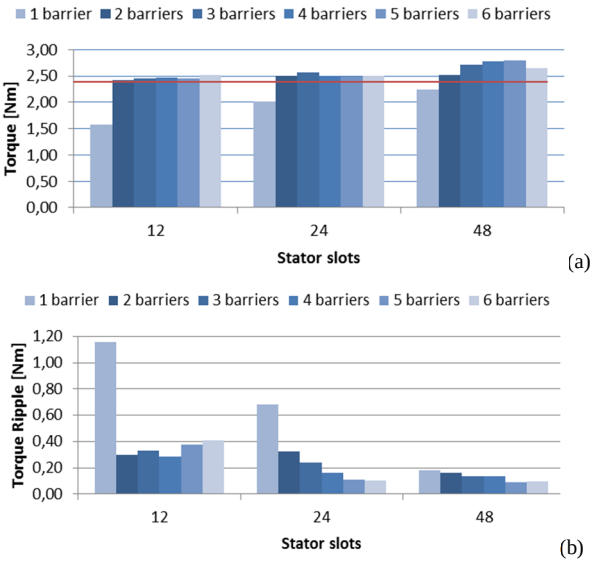

Fig. 7. Average torque (a) and standard deviation of torque ripple (b) at rated current in flux weakening (8000rpm).

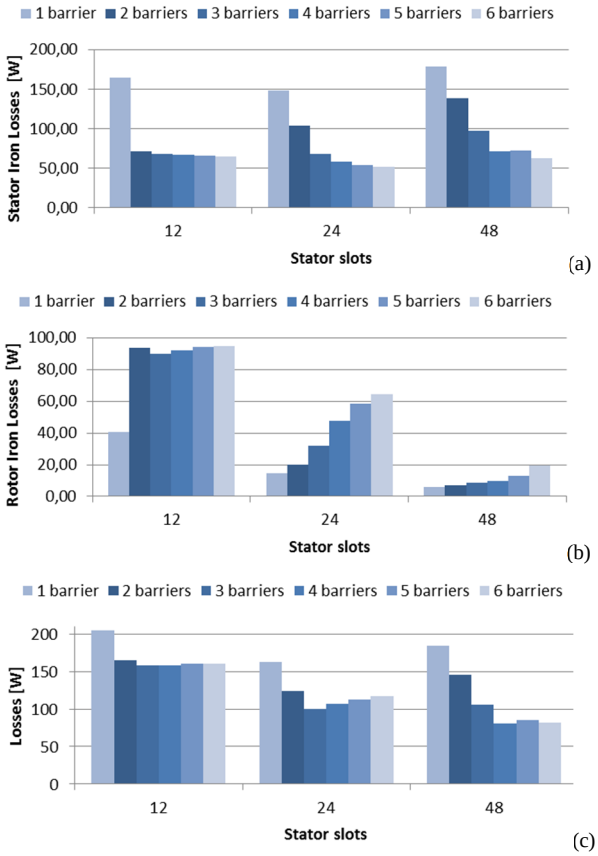

Fig. 8. Stator (a), rotor (b), and total (c) iron losses at rated current and 8000 rpm.

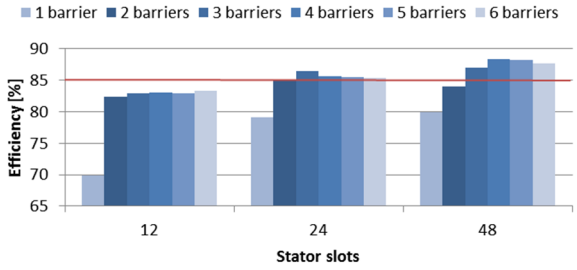

Fig. 9. Efficiency at rated current and 8000 rpm.

B. Iron Loss Results

Fig. 8 shows the iron losses in the stator and in the rotor cores of the 18 machines at 8000 rpm. For all examined cases, stator losses decrease when the number of rotor barriers increases, while the rotor losses have the opposite trend: hence, it is always possible to find a combination of rotor/stator slots that ensures a minimum value of total iron losses. As rotor losses are lower with the higher numbers of stator slots, their impact will generally play a role at higher layers numbers, for the higher slots numbers.

To make this point more clear, Fig. 8c reports the sum of stator and rotor iron losses. For each slot

number there is an optimal number of barriers that minimizes the total loss, and this number increases along with the slots number. For example, 12 and 24 slots stators must be associated to three barriers per pole rotors, while the 48 slots stator has minimum losses with the 4-layer rotor.

Finally, Fig. 9 reports the efficiency at 8000 rpm, rated current. Copper losses are the same for all the machines, but the torque is not the same for all. So, the higher efficiency is an aggregate indicator of better iron loss and higher torque capability, in this context.

C. Torque Ripple versus Iron Loss Minimization

A comparison between torque ripple and iron losses trends clearly shows that combinations of rotor/stator slots that minimize torque ripple do not guarantee the best efficiency and vice-versa, so it must be found a tradeoff between this two conflicting issues [13].

From Fig. 5b and Fig. 8 it can be noticed that, once the stator slots number is fixed and defining $n_{b,ripple}$ and $n_{b,loss}$ as rotor flux barriers numbers which minimize torque ripple and total iron losses respectively, it is always $n_{b,ripple} > n_{b,loss}$.

D. Conventional and Nonconventional MODE geometries

A selection of four optimized rotors is shown in Fig. 11, where for example 24/3 accounts for 24 slots and 3 barriers per pole. Figs. 10a, 10b, 10d show respectively stator and rotor laminations of machines 12/2, 24/3 and 48/4. The red circles identify the angular positions of the barriers ends that would be used according to the regular pitch criteria presented in [5], which are considered as the state of the art solution to minimize torque ripple. As stated in [5], for equally spaced rotor barriers, torque ripple can be minimized following the rule:

$$n_r = n_s \pm 4 \tag{5}$$

where n_s is the number of stator slots per pole pair and n_r is the number of equivalent rotor slots per pole pair.

With reference to the two pole pairs machines, three of the four examples in Fig. 10 follow the plus minus four rule.

In turn:

- Machine 12/2 → n_s = 6, $n_r = n_s + 4$ = 10 (i.e. 5 slots per rotor pole, 2 barriers plus a missing virtual slot on top of the *q*-axis, as in Fig. 11a);
- Machine 24/3 → n_s = 12, $n_r = n_s + 4$ = 16 (i.e. 8 rotor slots per pole, or 4 barriers. In Fig. 11b the three barriers are placed as they were four, and the smallest is missing);
- Machine 48/4 → n_s = 24, $n_r = n_s - 4$ = 20 (i.e. 10 rotor slots per pole, or 5 barriers. In Fig. 11d the four barriers are placed as they were five, and the smallest is missing).

Also in the state of the art designs the smallest barrier on top of the q-axis is often missing, for construction reasons.

Fig. 10c refers to a different type of solution with 24 slots and 5 layer, that can be considered a “non-conventional” one, according to the literature. As can be seen, in this case the automated design algorithm converged to a rotor geometry with 3 wide barriers spaced out by 2 thin inter-layers. The main barriers angular positions are similar to those of the “conventional” 24/3 motor (red circles) but machine 24/5 guarantees an average torque improvement of 3% and a torque ripple reduction of 47% with respect to machine 24/3.

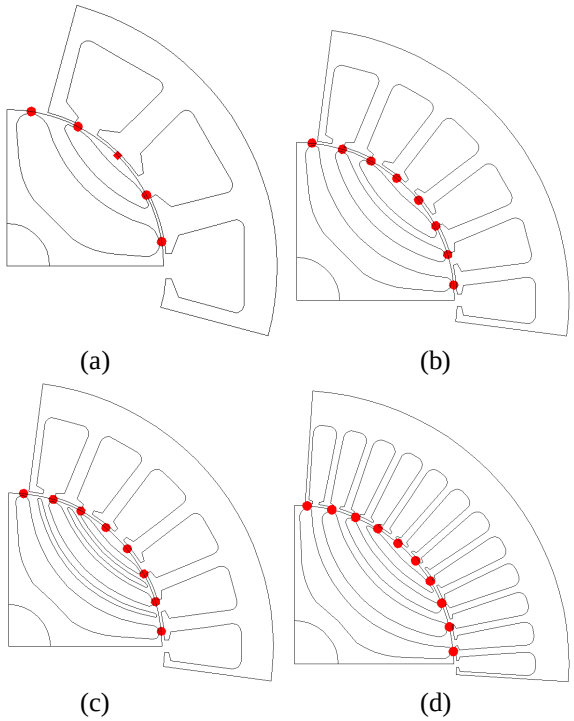

Fig. 10. Stator and rotor laminations of machines 12/2 (a), 24/3 (b), 24/5 (c), and 48/4(d).

E. Torque analysis in time and frequency domains

Figures 11 to 14 show the torque waveforms and the harmonic spectra of the just described machines 12/2, 24/3, 24/5 and 48/4, both at rated speed (first row) and at maximum speed (second row). As expected, each torque spectrum presents torque ripple components due to slots harmonics whose order is n_s and its multiples. Other harmonic components are due to the interaction between stator and rotor MMFs.

Comparing Fig. 12 and Fig. 13, it can be noticed that the "non-conventional" stator/rotor slots combination (24/5) produces a higher mean torque value at rated speed and lower torque harmonic content. This can be attributed to the presence of the two thin inter-layers which adds more degrees of freedom to the optimization process.

As reported in section III-A, a high number of stator slots is useful to reduce the harmonic content of torque profile. In the constant power region harmonic absolute amplitudes tend to grow but their relative amplitude is almost constant.

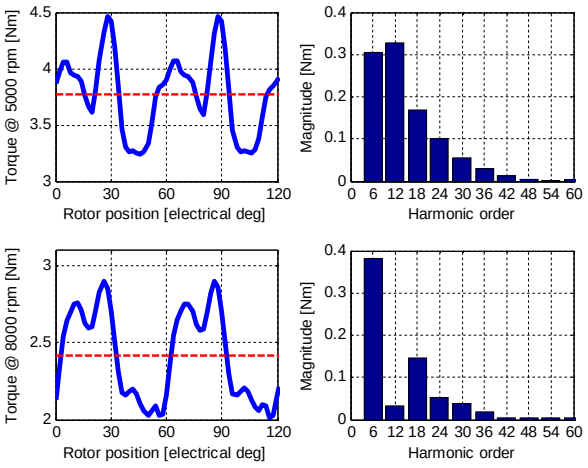

Fig. 11. Machine 12/2: torque versus rotor position and torque spectrum at 5000 rpm (1st row), 8000 rpm (2nd row)

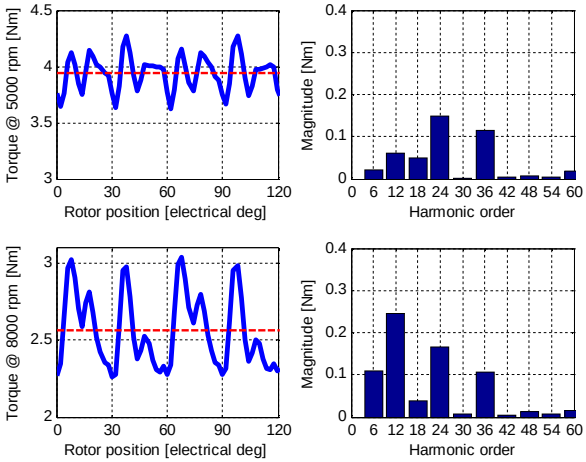

Fig. 12. Machine 24/3: torque versus rotor position and torque spectrum at 5000 rpm (1st row), 8000 rpm (2nd row)

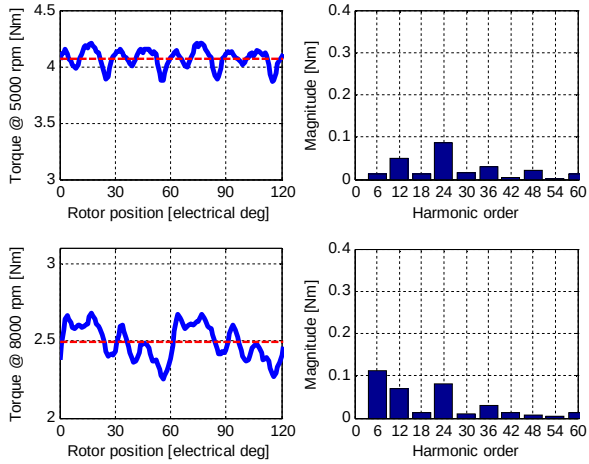

Fig. 13. Machine 24/5: torque versus rotor position and torque spectrum at 5000 rpm (1st row), 8000 rpm (2nd row)

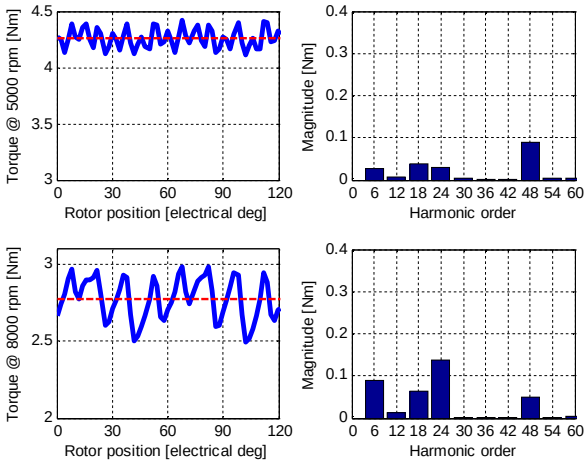

Fig. 14. Machine 48/4: torque versus rotor position and torque spectrum at 5000 rpm (1st row), 8000 rpm (2nd row)

IV. CONCLUSION

This paper presented a comparative study of the performances of synchronous reluctance machines considering different combinations of stator slots and flux barrier numbers. Eighteen different machines were designed via an automatic design procedure using DE optimization. Average torque, torque ripple and iron losses have been considered as the base for the comparison. Although some of the best slots/barriers combinations could be predicted using criteria suggested in the related literature, the presented analysis put in evidence that unconventional combination could improve the machine performances. Moreover it is shown that minimum torque ripple and minimum losses are somehow conflicting objectives. The optimal choice for slots and barriers numbers depends on the specific application and the presented results can be used as general design guidelines to find the most appropriate compromise between losses and torque ripple, and loss distribution between stator and rotor.

ACKNOWLEDGMENTS

This work was supported in part by project PON MALET – code PON01_01693.

REFERENCES

1. Staton, D.A., Miller, T.J.E., Wood, S.E.: *Maximising the saliency ratio of the synchronous reluctance motor*. In: Electric Power Applications, IEE Proceedings B , vol.140, no.4, pp.249,259, Jul 1993.
2. Lipo, T.A., Miller, T. J. E., Vagati, A., Boldea, I., Malesani, L., Fukao, T.: *Synchronous reluctance drives*. In: Conf. Rec. IEEE IAS Annu. Meeting, Denver, CO, Oct. 1994.
3. Kamper, M.J., Van der Merwe, F.S., Williamson, S.: *Direct finite element design optimisation of the cageless reluctance synchronous machine*. In: Energy Conversion, IEEE Transactions on , vol.11, no.3, pp.547-555, Sep 1996.
4. Boldea, I.: *Reluctance synchronous machines and drives*. Oxford, UK: Clarendon Press, 1996.
5. Vagati, A., Pastorelli, M., Francheschini, G., Petrache, S.C.: *Design of low-torque-ripple synchronous reluctance motors*. In: Industry Applications, IEEE Transactions on , vol.34, no.4, pp.758-765, Jul/Aug 1998.
6. Moghaddam, R.R.: *Rotor for a Synchronous Reluctance Machine*. WIPO Patent No. 2010102671. 17 Sep. 2010.
7. Vagati, A., Canova, A., Chiampi, M., Pastorelli, M., Repetto, M.: *Design refinement of synchronous reluctance motors through finite-element analysis*. In: Industry Applications, IEEE Transactions on , vol.36, no.4, pp.1094,1102, Jul/Aug 2000.
8. Pellegrino, G., Cupertino, F., Gerada, C.: *Barriers shapes and minimum set of rotor parameters in the automated design of Synchronous Reluctance machines*. In: Electric Machines & Drives Conference (IEMDC), 2013 IEEE International, vol., no., pp.1204,1210, 12-15 May 2013.
9. Pellegrino G., Cupertino F., Gerada C.: *Design of synchronous reluctance machines with multi-objective optimization algorithms*. In: IEEE Energy Conversion Congress and Exposition (ECCE), pp. 1858-1865, 2013
10. Wang, K., Zhu, Z.Q., Ombach, G., Koch, M., Zhang, S., Xu, J.: *Optimal Slot/Pole and Flux-Barrier Layer Number Combinations for Synchronous Reluctance Machines*. In: Ecological Vehicles and Renewable Energies (EVER), 2013 8th International Conference and Exhibition on, 2013, vol., no., pp.1-8, 27-30 March 2013.
11. Chalmers, B.J., Musaba, L.: *Design and field-weakening performance of a synchronous reluctance motor with axially laminated rotor*. In: Industry Applications, IEEE Transactions on , vol.34, no.5, pp.1035,1041, Sep/Oct 1998.
12. Hofmann, H., Sanders, S.R.: *High-speed synchronous reluctance machine with minimized rotor losses*. In: Industry Applications, IEEE Transactions on , vol.36, no.2, pp.531,539, Mar/Apr 2000.
13. Pellegrino, G., Guglielmi, P., Vagati, A., Villata, F.: *Core Losses and Torque Ripple in IPM Machines: Dedicated Modeling and Design Tradeoff*. In: Industry Applications, IEEE Transactions on , vol.46, no.6, pp.2381,2391, Nov.-Dec. 2010.
14. Seok-Hee Han, Jahns, T.M., Zhu, Z.Q.: *Analysis of Rotor Core Eddy-Current Losses in Interior Permanent-Magnet Synchronous Machines*. In: Industry Applications, IEEE Transactions on , vol.46, no.1, pp.196,205, Jan.-feb. 2010.
15. Seok-Hee Han, Jahns, T.M., Zhu, Z.Q.: *Design Tradeoffs Between Stator Core Loss and Torque Ripple in IPM Machines*. In: Industry Applications, IEEE Transactions on , vol.46, no.1, pp.187,195, Jan.-feb. 2010.
16. Binns, K.J., Laerenson, P.J., Trowbridge, C.W.: *The analytical and numerical solution of electric and magnetic fields*. New York: Wiley, 1992.
17. Meeker, D.: *Finite Element Method Magnetics*. Ver. 4.2 User's Manual, February 5, 2009, [Online] available: http://www.femm.info/Archives/doc/manual.pdf.
18. http://www.infolytica.com